Self-Organized Critical Coexistence Phase in Repulsive Active Particles

Xia-qing Shi,[1,2] Giordano Fausti,[2] Hugues Chaté,[2,3,4] Cesare Nardini,[2,4] and Alexandre Solon[4]

[1]*Center for Soft Condensed Matter Physics and Interdisciplinary Research, Soochow University, Suzhou 215006, China*
[2]*Service de Physique de l'Etat Condensé, CEA, CNRS Université Paris-Saclay, CEA-Saclay, 91191 Gif-sur-Yvette, France*
[3]*Computational Science Research Center, Beijing 100193, China*
[4]*Sorbonne Université, CNRS, Laboratoire de Physique Théorique de la Matière Condensée, 75005 Paris, France*

We revisit motility-induced phase separation in two models of active particles interacting by pairwise repulsion and uncover new qualitative features: the resulting dense phase contains gas bubbles distributed algebraically up to a typically extremely large cutoff scale. At large enough system size and/or global density, all the gas may be contained inside the bubbles, at which point the system is microphase separated with a finite cutoff bubble scale. We further observe that the ordering is clearly anomalous, with different dynamics for the coarsening of the dense phase and of the gas bubbles. This self-organized critical phenomenology is reproduced by a "reduced bubble model" that implements the basic idea of reverse Ostwald ripening put forward in Tjhung *et al.* [Phys. Rev. X **8**, 031080 (2018)].

Self-propelled particles interacting solely with steric repulsion are well known to be able to spontaneously separate into a macroscopic dense cluster and a residual gas, in spite of the absence of explicit attraction forces. This motility-induced phase separation (MIPS) [1] of active particles has become a cornerstone of the physics of dry active matter (in which the fluid surrounding particles is neglected). As such, it has driven many theoretical works [2–7] as well as countless numerical studies (see, e.g., Refs. [8–15], to name a few prominent ones). The motility reduction resulting from persistent collisions, which leads to MIPS, is a generic ingredient encountered in both living and synthetic active matter [16–19].

Despite its purely nonequilibrium origin, MIPS was initially described as a conventional phase separation between two homogeneous macroscopic phases. It was first predicted in models of quorum-sensing particles [2] where particle speed decreases with the local density, without two-body interactions. In this case, equilibriumlike thermodynamics can be constructed to account quantitatively for phase coexistence [20]. For systems of repulsive disks, attempts were made to model the speed reduction due to collisions by a quorum-sensing interaction [3,8,10], but the results are not satisfactory, due to fundamental differences between the two cases [5,21].

There is indeed mounting evidence that more complex physics is at play in systems of repulsive disks. In particular, the surface tension between the dense phase and the gas, defined via the Laplace law, has been measured to be negative [20,22,23], triggering a spate of controversy [24]. This was rationalized at field theoretical level by including terms that break detailed balance in the classical theory for equilibrium liquid-gas phase separation. In this active model B+ (AMB+), surface tension can become negative for some parameter values, in which case Ostwald ripening is reversed for vapor bubbles while still remaining normal for liquid droplets. This means that small vapor bubbles, contrary to the standard scenario, grow at the expense of larger ones due to a diffusion flux. When this happens, simulations of AMB+ lead to either a bubbly fluid interpreted as microphase separation or to the coexistence of a dense phase populated of bubbles with an outer gas [7]. There is in fact incidental evidence for such a bubbly liquid at particle level [9,11,12,20,22], but it has not yet been studied *per se*. Very recently, Caporusso *et al.* [27] have shown more clearly that in systems with hard-core interactions, the dense phase is made of hexatic subdomains and interstitial gas regions.

In this Letter we show, within two standard particle models displaying MIPS, that not only the dense phase is generically endowed with bubbles, but also that these are distributed algebraically up to some cutoff scale that we observe to grow with system size. The dense phase is thus a self-organized critical fluid, something heretofore unsuspected. Finite-size scaling based on this observation suggests that, as system size increases, more and more of the gas is contained in bubbles. At large densities, we are able to observe the vanishing of the macroscopic gas reservoir, and the system is then microphase separated with bubbles of all sizes up to a maximal bubble size that depends on the average density. Moreover, the coarsening of bubbles is anomalous with the typical length scale growing as $t^{0.22}$. We elucidate the basic mechanisms at play, and show, within a reduced model implementing reversed Ostwald ripening for gas bubbles, that they indeed lead to a self-organized critical dynamics.

Self-organized critical phase coexistence.—We first consider the paradigmatic active Brownian particles (ABPs) introduced in Ref. [8]. Self-propelled by a force of constant magnitude F_0 along its internal polarity $\mathbf{u}_i = (\cos\theta_i, \sin\theta_i)$, particle i evolves according to the overdamped Langevin equations governing its position $\mathbf{r}_i$ and polar angle θ_i:

$$\dot{\mathbf{r}}_i = \boldsymbol{\mu}_i(F_0\mathbf{u}_i + \mathbf{F}_i) + \boldsymbol{\eta}_i, \qquad \dot{\theta}_i = \eta_i, \qquad (1)$$

where $\mathbf{F}_i = -\sum_{j\neq i}\nabla V(\mathbf{r}_i - \mathbf{r}_j)$ is the force exerted on particle i by the other particles. We choose the pair potential to be a short-range harmonic repulsion $V(r) = (k/2)(\sigma - r)^2$ if $r < \sigma$ and 0 otherwise, with k the repulsive strength and $\sigma = 1$ the interaction radius. In contrast to previous studies, we allow the mobility tensor $\boldsymbol{\mu}_i$ and the translational noise $\boldsymbol{\eta}_i$ to be anisotropic, as expected generically for active particles: $\boldsymbol{\mu}_i = \mu_\parallel\mathbf{u}_i\mathbf{u}_i + \mu_\perp(\mathbf{I} - \mathbf{u}_i\mathbf{u}_i)$, $\boldsymbol{\eta}_i = \sqrt{2\tau\mu_\parallel}\xi_i^\parallel\mathbf{u}_i + \sqrt{2\tau\mu_\perp}\xi_i^\perp(\mathbf{u}_i \times \mathbf{z})$, and $\eta_i = \sqrt{2\tau\mu_\theta}\xi_i^\theta$, with τ a parameter controlling the noise strength, $\mathbf{z}$ the unit vector perpendicular to the plane of motion, and the ξ_i's Gaussian white noises with unit variance.

All simulations below are of large two-dimensional domains with periodic boundary conditions. Numerical details are given in Ref. [28]. At phase coexistence, we observe, inside the macroscopic dense domain, persistent bubbles with a range of sizes, surrounded by a liquid [29]. Bubbles are more prominent when the mobility is anisotropic [30]. Typical snapshots for $\mu_\parallel = 4\mu_\perp$ and $\mu_\theta = 6\mu_\perp$ are shown in Figs. 1(a) and 1(b) for systems only differing by their size. Clearly, doubling system size increases the size of the bubbles. Figure 1(c) shows, at different system sizes, $n(a)$, the average number of bubbles of area a, normalized by S_ℓ, the total area of the liquid in which bubbles live. The distributions collapse on an increasing range, span several orders of magnitude, and decay
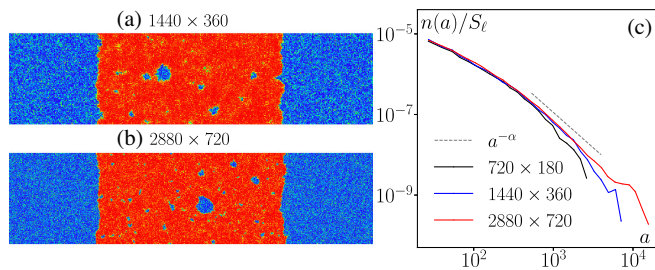

FIG. 1. Active Brownian particles. Typical snapshots in steady state at system size $S = 1440 \times 360$ (a) and $S = 2880 \times 720$ (b). [Colors represent the packing fraction calculated over 2×2 boxes, from 0 (dark blue) to 1 (red).] (c) Rescaled distribution of bubble area $n(a)/S_\ell$ at various system sizes (indicated in legends). Parameters are $\rho_0 = N\pi/4S = 0.6$, $\tau = 0.01$, $\mu_\perp = 1/4$, $\mu_\parallel = 1$, $\mu_\theta = 3/2$, $F_0 = 1$, and $k = 20$. Typical averaging time is 4×10^6 after a transient of 10^6.

approximately as a power law $n(a) \sim a^{-\alpha}$ with $\alpha \approx 1.75$ terminated by a cutoff that *increases* with system size.

The ABP simulations reported above only show a rather short scaling range. Numerically, the main limitation is not so much system size than the huge times needed to obtain clean averages [31]. We thus implemented an active lattice gas [32–36]: on a hexagonal lattice [36], particles carrying an internal polarity pointing to one of the six lattice directions attempt to perform one of three moves (see Ref. [28] for details). (i) With a rate r_P they perform a "self-propelled" jump to the nearest site along their internal polarity direction. (ii) They undergo spatial diffusion to any neighboring site at rate r_D and (iii) rotational diffusion (changing their polarity to one of its two neighboring orientations) at rate r_R. For optimal efficiency, we impose strict exclusion and parallel updating.

In the following, we use $r_P = 1$, $r_D = 2$, and $r_R = 0.032$, typical values leading to phase separation (a study of the phase diagram will be presented elsewhere). Persistent bubbles are clearly visible [Figs. 2(a)–2(d)]. The bubble area distribution in the globally phase-separated regime is similar to that observed for ABPs but with a much larger scaling region [Fig. 2(e)]: $n(a) \propto a^{-\alpha}$ with $\alpha = 1.75(5)$. This region extends to a cutoff size a_c that grows with the total liquid area as $a_c \propto S_\ell^\gamma$ with $\gamma = 1.40(5)$. The distributions can thus be collapsed on a master curve using these two exponents [Fig. 2(f)].

In both models presented, we find that whenever the system is globally phase separated, the dense phase contains bubbles. This phase bears the hallmarks of self-organized criticality (SOC) (for recent overviews, see Refs. [37,38]). Small bubbles are nucleated inside the liquid, diffuse, and grow by merging with other bubbles. This process gets slower and slower with increasing bubble size. Bubbles are eventually expelled into the reservoir of outside gas upon touching the boundary, in sudden, avalanchelike events, providing separation of timescales (see movie in Ref. [28]). As in typical SOC systems, avalanches occur at all accessible scales.

The SOC-like mechanisms leading to an algebraic distribution of bubbles do *not* invalidate the global picture of a phase separation between gas and liquid with fixed densities ρ_g and ρ_ℓ independent of system size up to small finite-size corrections. However, the gaseous part of the system is formed here of the outside gas reservoir *and* of the bubbles. With this definition, the gas fraction x_g fluctuates very little and is independent of system size to a good approximation [Fig. 3(a)]. Moreover, x_g varies linearly with the average density ρ_0 [Fig. 3(b)] so that the lever rule still applies: For $\rho_g < \rho_0 < \rho_\ell$, the average density sets the fraction of liquid and gas in the system $x_g = (\rho_\ell - \rho_0)/(\rho_\ell - \rho_g)$ and $x_\ell = 1 - x_g$. The fluctuations of x_b, the fraction of the system occupied by bubbles, in contrast to the gentle ones of x_g, are large, intermittent, and increase with system size. [Note the huge timescales
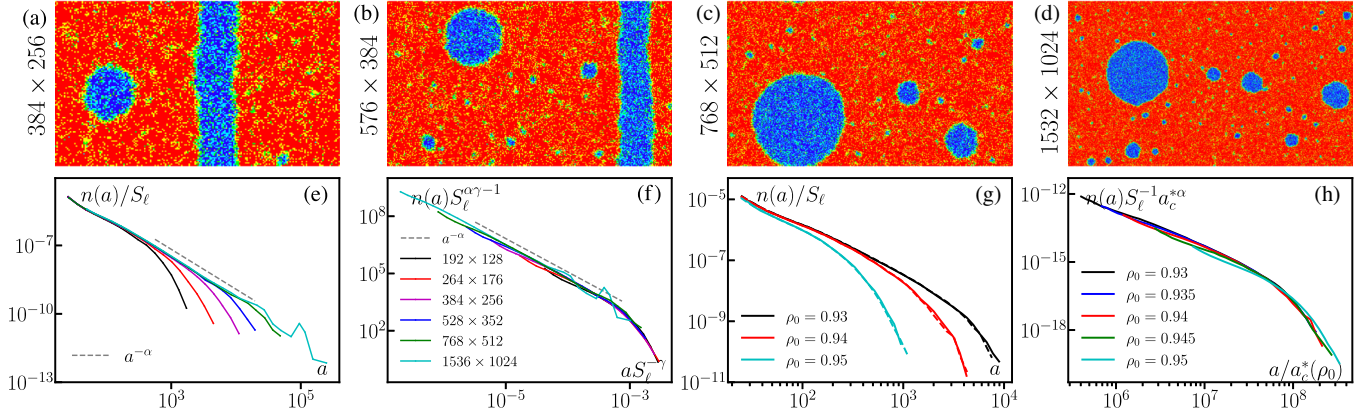
FIG. 2. Active lattice gas. (a)–(d) Snapshots in the steady state at $\rho_0 = 0.8$ in systems of different sizes from $S = 384 \times 256$ to $S = 1532 \times 1024$ [colors as in Figs. 1(a) and 1(b)]. For the two biggest sizes (c),(d), the system is in the microphase-separated regime. (e)–(h) Bubble area distribution in the SOC scaling regime [(e),(f) $\rho_0 = 0.6$] and in the microphase-separated regime (g),(h). (e) $n(a)/S_\ell$ at various system sizes [indicated by the legends in (f)]. Typical averaging time is 10^{10} time steps after discarding a transient of 10^8. (f) Same as (e), but as function of a/S_ℓ^γ with $\gamma = 1.40$. (g) $n(a)/S_\ell$ at different ρ_0 values for $S = 768 \times 1024$ (dashed lines) and $S = 1536 \times 2048$ (solid lines). (h) Same as (g), but rescaled according to Eq. (3). The gray dashed lines have slope $-\alpha = -1.75$.

over which fluctuations of x_b occur even at the modest sizes shown in Fig. 3(a).] Their stronger and stronger peaks reflect the larger and larger avalanches (expulsion of bubbles) [Fig. 3(a), insets].

Microphase-separated bubbly liquid.—The lever rule immediately tells us that the SOC scaling evidenced above cannot continue asymptotically when system size $S \to \infty$. Indeed, the bubble area fraction grows with system size:

$$x_b \equiv \frac{1}{S}\int_0^\infty a\,n(a)\,da \approx \frac{S_\ell}{S}\int_0^{a_c} a^{1-\alpha}\,da \propto x_\ell S_\ell^{\gamma(2-\alpha)}, \quad (2)$$

where we used the scalings of $n(a)$ and $a_c(S_\ell)$. Our numerical data confirm this [Fig. 3(c)]. Surely, Eq. (2)
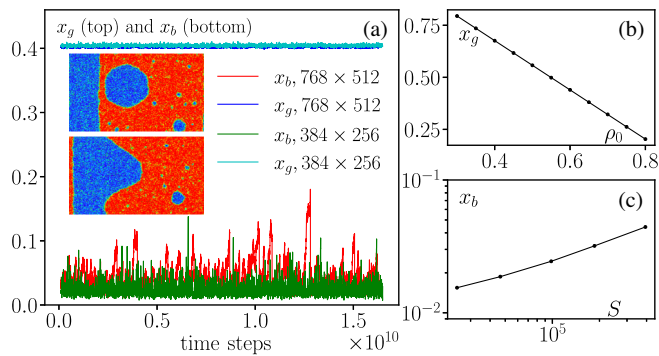

FIG. 3. Active lattice gas at $\rho_0 = 0.63$. (a) Time series of the area fraction occupied by bubbles x_b (bottom) and by total gas x_g (top) for system sizes $S = 384 \times 256$ and $S = 768 \times 512$. Insets: two snapshots of the system taken right before and at the sharpest peak in the x_b time series at $S = 768 \times 512$ (red curve, around $t = 1.3 \times 10^{10}$). (b) Linear variation of x_g with ρ_0 (lever rule) computed for $S = 384 \times 256$. (c) Bubble fraction x_b vs system size S.

ceases to be possible once all the gas is contained in the bubbles, $x_b = x_g$, which happens at a typical crossover size $S^* \propto (x_g/x_\ell)^{1/[\gamma(2-\alpha)]}/x_\ell$. The cutoff on bubble size then reads

$$a_c^* \equiv a_c(S^*) \propto (x_g/x_\ell)^{1/(2-\alpha)}. \quad (3)$$

Equation (3) implies that S^* and a_c^* depend on the average density ρ_0 through x_g and x_ℓ and that they diverge near the gas binodal $\rho_0 \to \rho_g$. On the other hand, they get smaller when approaching the liquid binodal. Beyond S^* the system settles in a microphase-separated state, a homogeneous liquid with bubbles of all sizes up to a_c^*. SOC scaling then breaks down, and $n(a)$ becomes independent of system size.

Using our lattice gas model at high enough ρ_0, we are able to reach system sizes where all the gas is contained in bubbles, and the system settles in the microphase-separated state (Fig. 2). The data are in agreement with our scaling arguments: $n(a)$ is then independent of system size and is cut off at some scale that depends only on the average density [Fig. 2(g)]. Plotting $n(a/a_c^*)$ collapses the distributions for different ρ_0, confirming the validity of Eq. (3) [Fig. 2(h)], at least close to the liquid binodal.

Reduced bubble model.—The AMB+ field theory of Ref. [7] suggests that bubbles exist because of reverse Ostwald ripening, which causes large bubbles to shrink at the advantage of small ones, thus competing with coalescence. To test whether these ingredients are sufficient to reproduce the phenomenology described above, we implemented them in a reduced model whose degrees of freedom are the positions and radii of bubbles that we assume to be perfectly circular [39].

The bubble particles evolve in continuous time in a continuous domain. New bubbles with radius $r_0 = 1$ are

nucleated in the liquid at a small rate k_n per unit area. In line with the reverse Ostwald scenario, the new bubbles are nucleated at the expense of the larger ones: all other bubbles shrink by an amount $\kappa r(1 - r_0/r)$ (where r is their current radius), with κ chosen such that the total area of gas is conserved. (Note that this neglects spatial effects: In principle, bubbles would equilibrate in priority with neighboring ones.) Bubbles chosen randomly among the current $n(t)$ existing ones diffuse with a coefficient D, that for simplicity we assume constant. If the move brings the bubble into contact with another, they merge into a single one located at their "center of mass," conserving total area. To have the same geometry as in globally phase-separated microscopic models, we also add the possibility to have a gas reservoir outside two parallel interfaces that move along the dynamics to ensure that x_ℓ remains constant.

While a complete presentation of the behavior of this reduced model and some variants will be reported elsewhere, here we show that it typically yields a phenomenology remarkably similar to that described above. Fixing $D = 1$ and $k_n = 10^{-4}$, we vary x_g, the total gas fraction, and the system size S. At high x_g or small system size S, we observe the SOC coexistence between a bubbly liquid and a gas reservoir [Figs. 4(a) and 4(b)]. The bubble size distribution scales as in Fig. 2(f) with exponent values close to those of the lattice gas [$\alpha = 1.77(2)$ and $\gamma = 1.48(5)$], but preliminary results (not shown) suggest that they are not universal. Decreasing x_g or increasing S, the gas reservoir becomes smaller and smaller until it disappears, at which point we have a microphase-separated regime with $n(a)$ independent of system size [Figs. 4(c) and 4(d)]. Despite its simplicity, our bubble model thus captures the essential phenomenology described here.
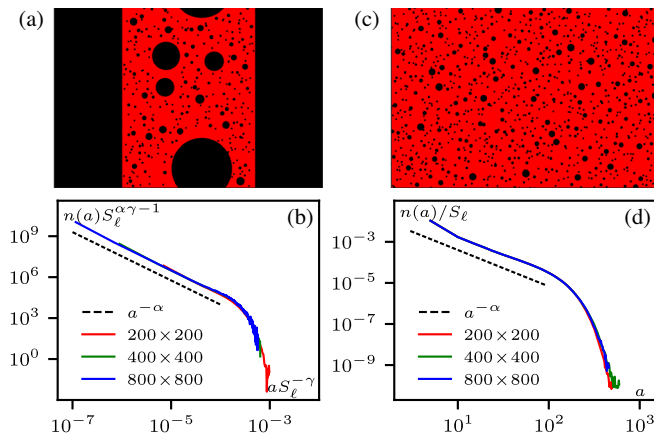

FIG. 4. Reduced bubble model. (a),(c) Typical snapshots at $x_g = 0.7$ in the SOC coexistence regime (a) and at $x_g = 0.05$ in the microphase regime (c). System size $S = 600 \times 400$. The liquid and gas are represented in red and black, respectively. (b),(d) Bubble area distribution in the two regimes, rescaled using $\alpha = 1.77$, $\gamma = 1.48$. For all panels, $D = 1$, $k_n = 10^{-4}$.
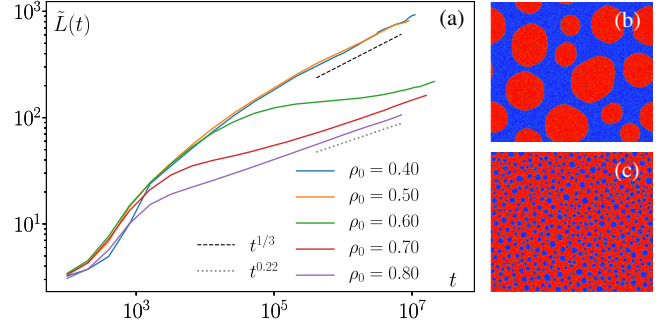

FIG. 5. Coarsening process in the active lattice gas ($S = 8192 \times 6144$). (a) Time series of the typical length scale $\tilde{L}$ starting from random initial conditions at different ρ_0 values. (b),(c) Snapshots of the system taken at $t = 10^7$ for $\rho_0 = 0.5$ (b) and 0.7 (c). At all times shown here, $\tilde{L} \ll \sqrt{S}$.

Coarsening process.—We finally study the growth of order following random initial conditions, considering the characteristic length extracted from the structure factor [28]. We only present results for our active lattice gas (Fig. 5), but similar ones, albeit of lesser quality, were obtained for ABPs. When the liquid is the majority phase, after an initial transient, the coarsening is dominated by vapor bubbles and follows an anomalous $t^{0.22}$ law. We currently lack an analytical explanation of such law. Instead, when the liquid is the minority phase, it is dominated by liquid droplets and coarsening is normal $t^{1/3}$ as expected both from Ostwald ripening and coalescence in models with conserved order parameter [41]. In fact, within the liquid droplets we expect the bubbles to coarsen as well with the anomalous law above. However, being slower than the liquid coarsening, it is not surprising that this is not visible in our data.

Conclusion.—We have shown, using two very different models of active particles interacting strictly by pairwise repulsion, that the dense phase resulting from MIPS is critical, containing bubbles of gas distributed algebraically up to some cutoff scale. We observe at high density that, as long as an outer gas phase is present, this cutoff increases as a power of system size. At large enough system size and/or global density, the gas reservoir may disappear and the cutoff scale becomes independent of system size. This asymptotic regime is thus microphase separated. A "reduced bubble model" captures this essential phenomenology within a minimal framework that implements the basic idea of reverse Ostwald ripening put forward in Ref. [7].

In the models presented here, the asymptotic cutoff scale a_c^* grows very fast as ρ_0 departs from ρ_ℓ. Numerically, we are only able to access the asymptotic regime at rather high density (Fig. 2). What happens asymptotically at low densities thus remains unknown, but extrapolating the scaling laws uncovered here leads us to speculate that our scenario remains valid in the whole phase coexistence region $\rho_g < \rho_0 < \rho_\ell$.

This Letter leaves several important open questions. In particular, whether the scenario described here is observed in the presence of any repulsion and whether the critical exponents are universal could be addressed numerically by considering other models showing MIPS, the AMB+ field theory, and reduced bubble models with different parameters. In this context, the very recent work of Caporusso et al. [27], where a very hard potential between ABPs leads to crystalline clusters that aggregate to form a dense phase with interstitial gas, might be understood within our scenario. Finally, in regard to the current controversy about the nature of the critical point of MIPS [36,42], our results make it unlikely that it belongs to the Ising universality class, but this hard problem remains unsettled.

[1] M. E. Cates and J. Tailleur, Motility-induced phase separation, Annu. Rev. Condens. Matter Phys. 6, 219 (2015).

[2] J. Tailleur and M. E. Cates, Statistical Mechanics of Interacting Run-and-Tumble Bacteria, Phys. Rev. Lett. 100, 218103 (2008).

[3] J. Stenhammar, A. Tiribocchi, R. J. Allen, D. Marenduzzo, and M. E. Cates, Continuum Theory of Phase Separation Kinetics for Active Brownian Particles, Phys. Rev. Lett. 111, 145702 (2013).

[4] R. Wittkowski, A. Tiribocchi, J. Stenhammar, R. J. Allen, D. Marenduzzo, and M. E. Cates, Scalar ϕ^4 field theory for active-particle phase separation, Nat. Commun. 5, 4351 (2014).

[5] A. P. Solon, J. Stenhammar, R. Wittkowski, M. Kardar, Y. Kafri, M. E. Cates, and J. Tailleur, Pressure and Phase Equilibria in Interacting Active Brownian Spheres, Phys. Rev. Lett. 114, 198301 (2015).

[6] A. P. Solon, J. Stenhammar, M. E. Cates, Y. Kafri, and J. Tailleur, Generalized thermodynamics of phase equilibria in scalar active matter, Phys. Rev. E 97, 020602(R) (2018).

[7] E. Tjhung, C. Nardini, and M. E. Cates, Cluster Phases and Bubbly Phase Separation in Active Fluids: Reversal of the Ostwald Process, Phys. Rev. X 8, 031080 (2018).

[8] Y. Fily and M. C. Marchetti, Athermal Phase Separation of Self-Propelled Particles with No Alignment, Phys. Rev. Lett. 108, 235702 (2012).

[9] G. S. Redner, M. F. Hagan, and A. Baskaran, Structure and Dynamics of a Phase-Separating Active Colloidal Fluid, Phys. Rev. Lett. 110, 055701 (2013).

[10] T. Speck, J. Bialké, A. M. Menzel, and H. Löwen, Effective Cahn-Hilliard Equation for the Phase Separation of Active Brownian Particles, Phys. Rev. Lett. 112, 218304 (2014).

[11] J. Stenhammar, D. Marenduzzo, R. J. Allen, and M. E. Cates, Phase behaviour of active Brownian particles: The role of dimensionality, Soft Matter 10, 1489 (2014).

[12] P. Digregorio, D. Levis, A. Suma, L. F. Cugliandolo, G. Gonnella, and I. Pagonabarraga, Full Phase Diagram of Active Brownian Disks: From Melting to Motility-Induced Phase Separation, Phys. Rev. Lett. 121, 098003 (2018).

[13] J. U. Klamser, S. C. Kapfer, and W. Krauth, Thermodynamic phases in two-dimensional active matter, Nat. Commun. 9, 5045 (2018).

[14] S. Mandal, B. Liebchen, and H. Löwen, Motility-Induced Temperature Difference in Coexisting Phases, Phys. Rev. Lett. 123, 228001 (2019).

[15] L. Caprini, U. Marini Bettolo Marconi, and A. Puglisi, Spontaneous Velocity Alignment in Motility-Induced Phase Separation, Phys. Rev. Lett. 124, 078001 (2020).

[16] G. Liu, A. Patch, F. Bahar, D. Yllanes, R. D. Welch, M. C. Marchetti, S. Thutupalli, and J. W. Shaevitz, Self-Driven Phase Transitions Drive Myxococcus Xanthus Fruiting Body Formation, Phys. Rev. Lett. 122, 248102 (2019).

[17] I. Buttinoni, J. Bialké, F. Kümmel, H. Löwen, C. Bechinger, and T. Speck, Dynamical Clustering and Phase Separation in Suspensions of Self-Propelled Colloidal Particles, Phys. Rev. Lett. 110, 238301 (2013).

[18] D. Geyer, D. Martin, J. Tailleur, and D. Bartolo, Freezing a Flock: Motility-Induced Phase Separation in Polar Active Liquids, Phys. Rev. X 9, 031043 (2019).

[19] M. N. van der Linden, L. C. Alexander, D. G. A. L. Aarts, and O. Dauchot, Interrupted Motility Induced Phase Separation in Aligning Active Colloids, Phys. Rev. Lett. 123, 098001 (2019).

[20] A. P. Solon, J. Stenhammar, M. E. Cates, Y. Kafri, and J. Tailleur, Generalized thermodynamics of motility-induced phase separation: Phase equilibria, laplace pressure, and change of ensembles, New J. Phys. 20, 075001 (2018).

[21] A. P. Solon, Y. Fily, A. Baskaran, M. E. Cates, Y. Kafri, M. Kardar, and J. Tailleur, Pressure is not a state function for generic active fluids, Nat. Phys. 11, 673 (2015).

[22] J. Bialké, J. T. Siebert, H. Löwen, and T. Speck, Negative Interfacial Tension in Phase-Separated Active Brownian Particles, Phys. Rev. Lett. 115, 098301 (2015).

[23] A. Patch, D. M. Sussman, D. Yllanes, and M. C. Marchetti, Curvature-dependent tension and tangential flows at the interface of motility-induced phases, Soft Matter 14, 7435 (2018).

[24] Two recent papers either contest [25] or regard as physically irrelevant [26] that the surface tension is measured to be negative in numerical simulations.

[25] S. Hermann, D. de las Heras, and M. Schmidt, Non-negative Interfacial Tension in Phase-Separated Active Brownian Particles, Phys. Rev. Lett. 123, 268002 (2019).

[26] A. K. Omar, Z.-G. Wang, and J. F. Brady, Microscopic origins of the swim pressure and the anomalous surface tension of active matter, Phys. Rev. E 101, 012604 (2020).

[27] C. B. Caporusso, P. Digregorio, D. Levis, L. F. Cugliandolo, and G. Gonnella, Micro and macro motility-induced phase separation in a two-dimensional active Brownian

particle system, arXiv:2005.06893 [Phys. Rev. Lett. (to be published)].

[28] See Supplemental Material at http://link.aps.org/supplemental/10.1103/PhysRevLett.125.168001 for supplementary movies and numerical details.

[29] It is convenient to work at intermediate noise strength or Péclet number: too close to the critical region, interfaces are fuzzy, while at low noise bubble dynamics is even slower. We do not expect our results to change much with parameters.

[30] With isotropic mobility bubbles exist, but are rather rare and small at the sizes studied.

[31] This is illustrated in Fig. 3(a) for the other model studied here.

[32] A. G. Thompson, J. Tailleur, M. E. Cates, and R. A. Blythe, Lattice models of nonequilibrium bacterial dynamics, J. Stat. Mech. (2011) P02029.

[33] R. Soto and R. Golestanian, Self-Assembly of Catalytically Active Colloidal Molecules: Tailoring Activity Through Surface Chemistry, Phys. Rev. Lett. **112**, 068301 (2014).

[34] N. Sepúlveda and R. Soto, Wetting Transitions Displayed by Persistent Active Particles, Phys. Rev. Lett. **119**, 078001 (2017).

[35] S. Whitelam, K. Klymko, and D. Mandal, Phase separation and large deviations of lattice active matter, J. Chem. Phys. **148**, 154902 (2018).

[36] B. Partridge and C. F. Lee, Critical Motility-Induced Phase Separation Belongs to the Ising Universality Class, Phys. Rev. Lett. **123**, 068002 (2019).

[37] G. Pruessner, *Self-Organised Criticality* (Cambridge University Press, Cambridge, 2012).

[38] V. Buendía, S. di Santo, J. A. Bonachela, and M. A. Muñoz, Feedback mechanisms for self-organization to the edge of a phase transition, arXiv:2006.03020.

[39] For a similar approach in a different context, see Ref. [40].

[40] J. Ranft, L. G. Almeida, P. C. Rodriguez, A. Triller, and V. Hakim, An aggregation-removal model for the formation and size determination of post-synaptic scaffold domains, PLoS Comput. Biol. **13**, e1005516 (2017).

[41] A. J. Bray, Theory of phase-ordering kinetics, Adv. Phys. **51**, 481 (2002).

[42] J. T. Siebert, F. Dittrich, F. Schmid, K. Binder, T. Speck, and P. Virnau, Critical behavior of active Brownian particles, Phys. Rev. E **98**, 030601(R) (2018).